SIAM J. NUMER. ANAL.
Vol. 45, No. 2, pp. 539–557

VARIATIONAL MULTISCALE ANALYSIS: THE FINE-SCALE GREEN'S FUNCTION, PROJECTION, OPTIMIZATION, LOCALIZATION, AND STABILIZED METHODS*

T. J. R. HUGHES† AND G. SANGALLI‡

Abstract. We derive an explicit formula for the fine-scale Green's function arising in variational multiscale analysis. The formula is expressed in terms of the classical Green's function and a projector which defines the decomposition of the solution into coarse and fine scales. The theory is presented in an abstract operator format and subsequently specialized for the advection-diffusion equation. It is shown that different projectors lead to fine-scale Green's functions with very different properties. For example, in the advection-dominated case, the projector induced by the H_0^1-seminorm produces a fine-scale Green's function which is highly attenuated and localized. These are very desirable properties in a multiscale method and ones that are not shared by the L^2-projector. By design, the coarse-scale solution attains optimality in the norm associated with the projector. This property, combined with a localized fine-scale Green's function, indicates the possibility of effective methods with local character for dominantly hyperbolic problems. The constructs lead to a new class of stabilized methods, and the relationship between H_0^1-optimality and the streamline-upwind Petrov-Galerkin (SUPG) method is described.

Key words. multiscale, advection-diffusion

AMS subject classification. 65N30

DOI. 10.1137/050645646

1. Introduction.

The variational multiscale (VMS) method [12, 13] was introduced as a framework for incorporating missing fine-scale effects into numerical problems governing coarse-scale behavior. It has provided a rationale for stabilized methods and a platform for the development of new methods (see, e.g., [11, 14, 15, 16, 18] for application to turbulence modeling). The fundamental mathematical object in the method is the so-called *fine-scale Green's function*, introduced in [13]. Although it is a simple matter to characterize coarse-scale and fine-scale subspaces, not much is known about the fine-scale Green's function. In this paper, we study the fine-scale Green's function and present a formula for explicitly computing it from the classical Green's function. This is accomplished by observing that the decomposition of a function into a sum of coarse-scale and fine-scale components is uniquely specified by identifying a projector from the space of all scales onto the coarse-scale subspace. Different projectors produce different decompositions. The problem for the fine-scale Green's function is then posed in terms of the fine-scale subspace. Compared with the problem for the classical Green's function, this amounts to a constrained formulation. The constraint can be released by invoking the Lagrange multiplier method and the unconstrained problem can be solved in terms of the classical Green's function and the projector. The fine-scale Green's function enjoys orthogonality relations with respect

*Received by the editors November 19, 2005; accepted for publication (in revised form) October 17, 2006; published electronically March 19, 2007.
http://www.siam.org/journals/sinum/45-2/64564.html

†Institute for Computational Engineering and Sciences, The University of Texas at Austin, Austin, TX 78712-0027 (hughes@ices.utexas.edu). The work of this author was supported by Sandia contract A0340.0 with the University of Texas and is gratefully acknowledged.

‡Dipartimento di Matematica, Università di Pavia, Via Ferrata 1, 27100 Pavia, Italy (sangalli@imati.cnr.it). This research of this author was supported by the J. Tinsley Oden Faculty Fellowship Research Program and PRIN 2004 project of the Italian MIUR.

to the projector. If a scalar product is introduced with a corresponding projector, the coarse-scale solution of the original problem is the optimal approximation in terms of the induced norm. The theory summarizing these ideas is presented in section 2 in an abstract operator format for a general linear isomorphism.

These ideas are applied to the advection-diffusion equation in section 3. The fine-scale Green's function is explicitly calculated in one dimension for linear, quadratic, and cubic finite elements when the projector is defined by the H_0^1-seminorm. In this case, the fine-scale Green's function is local in that it is confined to individual elements and is not coupled from one element to another, even in advection-dominated cases. This is a highly desirable property in multiscale analysis and in complete contrast with the classical Green's function which exhibits global support in advection-dominated cases. It also suggests that efficient, approximate, multiscale methods possessing local character may be possible for dominantly hyperbolic phenomena. On the other hand, selecting the L^2-projector results in a fine-scale Green's function with global coupling. These results show clearly that the choice of projector is of key importance in the development of a multiscale method.

The fine-scale Green's function becomes increasingly complicated as the order of the coarse-scale space is increased. However, it is observed that due to the orthogonality properties of the fine-scale Green's function, it only interacts with the highest-order polynomial term in the residual. This means that for a kth-order coarse-scale space, the fine-space Green's function modification to the coarse-scale equation can be replaced by an equivalent stabilization term involving a computable, elementwise constant (i.e., a "τ" in the notation of stabilized methods) and derivatives of the residual and weighting operator of order $k-1$. Remarkably, the modification reduces to elementwise constant terms requiring no quadrature despite the complexity of the fine-scale Green's function. This results in optimal higher-order methods of extraordinary simplicity.

To assess the situation in multiple dimensions, the two-dimensional advection-diffusion equation is studied. Here, rather than proceeding analytically, numerical procedures involving very fine meshes are utilized to determine Green's functions. As in the one-dimensional case, the classical Green's function exhibits global character with support in the form of a tail surrounding the upwind characteristic through the point of application of the Dirac mass. When advection-dominated, this tail is not attenuated with distance. However, the fine-scale Green's function for the H_0^1-projector is highly attenuated under the same circumstances and is essentially confined to a small number of elements (in the coarse-scale space) surrounding the point of application of the Dirac mass. The L^2-projector engenders a fine-scale Green's function which is not localized, and one concludes that the main observations made for the one-dimensional case are essentially true in two dimensions.

The H_0^1-projector produces a method which is highly localized and attains an optimal approximation in the H_0^1-seminorm, a combination of desirable properties. It is also noted that the modification it introduces to a classical Galerkin formulation involves an additional stabilization term in which the coarse-scale residual is weighted by the fine-scale Green's function convolved only with the advective part of the operator, i.e., the diffusive operator does not appear in the weighting. These are features that the H_0^1-optimal method has in common with streamline-upwind Petrov-Galerkin (SUPG) [9].

In section 4 we draw conclusions.

2. The abstract framework.

2.1. The abstract problem. Let V be a Hilbert space endowed with a norm $\|\cdot\|_V$ and a scalar product $(\cdot,\cdot)_V$. Let V^* be the dual of V, and let ${}_{V^*}\langle\cdot,\cdot\rangle_V$ be the pairing between them. Let $\mathcal{L} : V \to V^*$ be a linear isomorphism. Given $f \in V^*$, we consider the abstract problem of finding $u \in V$ such that

$$\mathcal{L}u = f. \tag{2.1}$$

The variational formulation of (2.1) is find $u \in V$ such that

$${}_{V^*}\langle \mathcal{L}u, v\rangle_V = {}_{V^*}\langle f, v\rangle_V \qquad \forall v \in V. \tag{2.2}$$

The solution u can be expressed as $u = \mathcal{G}f$, where $\mathcal{G} : V^* \to V$ is the Green's operator, i.e., $\mathcal{G} = \mathcal{L}^{-1}$.

2.2. The variational multiscale formulation. Let $\bar{V}$ be a closed subspace of V, and let $\mathcal{P}$ be a linear projector onto $\bar{V}$; i.e., $\mathcal{P}^2 = \mathcal{P}$ and $\mathrm{Range}(\mathcal{P}) = \bar{V}$. We assume $\mathcal{P}$ to be continuous in V. Since $\mathcal{P}\bar{v} = \bar{v}$ for all $\bar{v} \in \bar{V}$, we have the obvious inf-sup condition

$$\inf_{\bar{v}\in\bar{V}} \sup_{w\in V} \frac{(\mathcal{P}w, \bar{v})_V}{\|w\|_V \|\bar{v}\|_V} \geq 1. \tag{2.3}$$

We define $V' = \mathrm{Ker}(\mathcal{P})$, which is a closed subspace of V, thanks to the continuity of $\mathcal{P}$. As a consequence,

$$V = \bar{V} \oplus V'; \tag{2.4}$$

i.e., any $v \in V$ can be written uniquely as $v = \bar{v} + v'$, where $\bar{v} \in \bar{V}$ and $v' \in V'$: indeed, $\bar{v} = \mathcal{P}v$ and $v' = v - \mathcal{P}v$. In particular, we split the solution u of (2.1) as $u = \bar{u} + u'$. In the VMS approach, $\bar{V}$ represents the space of computable *coarse scales*, while V' contains the unresolved *fine scales*. The aim of the VMS approach is to obtain $\bar{u} = \mathcal{P}u$.

The variational formulation (2.2) splits into

$${}_{V^*}\langle \mathcal{L}\bar{u}, \bar{v}\rangle_V + {}_{V^*}\langle \mathcal{L}u', \bar{v}\rangle_V = {}_{V^*}\langle f, \bar{v}\rangle_V \qquad \forall \bar{v} \in \bar{V}, \tag{2.5}$$

$${}_{V^*}\langle \mathcal{L}\bar{u}, v'\rangle_V + {}_{V^*}\langle \mathcal{L}u', v'\rangle_V = {}_{V^*}\langle f, v'\rangle_V \qquad \forall v' \in V'. \tag{2.6}$$

We assume that (2.5) is a well-posed problem for $\bar{u}$ alone, meaning that it admits a unique solution $\bar{u} \in \bar{V}$ given u' and f. Analogously, we assume that (2.6) is well-posed for $u' \in V'$ given $\bar{u}$ and f. For that, we ask the inf-sup conditions for $\mathcal{L}$ on $\bar{V}$ and V'

$$\inf_{\bar{w}\in\bar{V}} \sup_{\bar{v}\in\bar{V}} \frac{{}_{V^*}\langle \mathcal{L}\bar{w}, \bar{v}\rangle_V}{\|\bar{w}\|_V \|\bar{v}\|_V} > 0 \quad \text{and} \quad \sup_{\bar{w}\in\bar{V}} \frac{{}_{V^*}\langle \mathcal{L}\bar{w}, \bar{v}\rangle_V}{\|\bar{w}\|_V} > 0 \quad \forall \bar{v} \in \bar{V}\backslash\{0\}, \tag{2.7}$$

$$\inf_{w'\in V'} \sup_{v'\in V'} \frac{{}_{V^*}\langle \mathcal{L}w', v'\rangle_V}{\|w'\|_V \|v'\|_V} > 0 \quad \text{and} \quad \sup_{w'\in V'} \frac{{}_{V^*}\langle \mathcal{L}w', v'\rangle_V}{\|w'\|_V} > 0 \quad \forall v' \in V'\backslash\{0\}. \tag{2.8}$$

If $\mathcal{L}$ is coercive on V, i.e., ${}_{V^*}\langle \mathcal{L}v, v\rangle_V \geq C\|v\|_V^2$ for $C > 0$ and for all $v \in V$, then (2.7)–(2.8) hold.

We associate with (2.6) the *fine-scale Green's operator* $\mathcal{G}' : V^* \to V'$, which gives u' from the coarse-scale *residual* $f - \mathcal{L}\bar{u}$, i.e.,

$$u' = \mathcal{G}'(f - \mathcal{L}\bar{u}). \tag{2.9}$$

Having $\mathcal{G}'$, we can eliminate u' from (2.5), and we obtain the VMS formulation for $\bar{u}$:

$$(2.10) \qquad {}_{V^*}\langle \mathcal{L}\bar{u}, \bar{v}\rangle_V - {}_{V^*}\langle \mathcal{L}\mathcal{G}'\mathcal{L}\bar{u}, \bar{v}\rangle_V = {}_{V^*}\langle f, \bar{v}\rangle_V - {}_{V^*}\langle \mathcal{L}\mathcal{G}' f, \bar{v}\rangle_V \qquad \forall \bar{v} \in \bar{V}.$$

Because of (2.4), the formulation (2.10) admits a unique solution, which is precisely $\bar{u} = \mathcal{P}u$.

2.3. The fine-scale Green's operator. We denote by $\mathcal{P}^T : \bar{V}^* \to V^*$ the adjoint of $\mathcal{P}$, i.e.,

$$ {}_{V^*}\langle \mathcal{P}^T\bar{\mu}, v\rangle_V = {}_{\bar{V}^*}\langle \bar{\mu}, \mathcal{P}v\rangle_{\bar{V}} \qquad \forall v \in V,\ \bar{\mu} \in \bar{V}^*,$$

where $\bar{V}^*$ is the dual of $\bar{V}$ and ${}_{\bar{V}^*}\langle\cdot,\cdot\rangle_{\bar{V}}$ is the pairing between them.

In the next result we express $\mathcal{G}'$ in terms of $\mathcal{G}$ and $\mathcal{P}$.

THEOREM 2.1. *Under the assumptions of sections* 2.1 and 2.2*, we have*

$$(2.11) \qquad \mathcal{G}' = \mathcal{G} - \mathcal{G}\mathcal{P}^T(\mathcal{P}\mathcal{G}\mathcal{P}^T)^{-1}\mathcal{P}\mathcal{G},$$

$$(2.12) \qquad \mathcal{G}'\mathcal{P}^T = 0, \quad \textit{and} \quad \mathcal{P}\mathcal{G}' = 0.$$

Proof. Since (2.6) is a constrained problem, we can rephrase it making use of a Lagrange multiplier in mixed (unconstrained) form: Find $u' \in V$ and $\bar{\lambda} \in \bar{V}^*$ such that

$$(2.13) \qquad \mathcal{L}u' + \mathcal{P}^T\bar{\lambda} = r,$$

$$(2.14) \qquad \mathcal{P}u' = 0,$$

where $r = f - \mathcal{L}\bar{u}$. The well-posedness of (2.13)–(2.14), for any $r \in V^*$, is guaranteed by our previous assumptions. Indeed, following [2], we need (2.8) and the inf-sup condition for $\mathcal{P}$

$$\inf_{\bar{\mu}\in\bar{V}^*} \sup_{w\in V} \frac{{}_{\bar{V}^*}\langle \bar{\mu}, \mathcal{P}w\rangle_{\bar{V}}}{\|\bar{\mu}\|_{\bar{V}^*}\|w\|_V},$$

which is equivalent to (2.3) in this Hilbert space setting. From (2.13) we get $u' = \mathcal{G}(r - \mathcal{P}^T\bar{\lambda})$; substituting in (2.14) gives $\mathcal{P}\mathcal{G}r - \mathcal{P}\mathcal{G}\mathcal{P}^T\bar{\lambda} = 0$; the well-posedness of (2.13)–(2.14) guarantees the invertibility of $\mathcal{P}\mathcal{G}\mathcal{P}^T$; and hence we obtain $\bar{\lambda} = (\mathcal{P}\mathcal{G}\mathcal{P}^T)^{-1}\mathcal{P}\mathcal{G}r$. Finally, using this in the expression for u' yields

$$(2.15) \qquad u' = (\mathcal{G} - \mathcal{G}\mathcal{P}^T(\mathcal{P}\mathcal{G}\mathcal{P}^T)^{-1}\mathcal{P}\mathcal{G})r,$$

which gives (2.11).

From (2.11), we immediately have

$$\mathcal{G}'\mathcal{P}^T = \mathcal{G}\mathcal{P}^T - \mathcal{G}\mathcal{P}^T(\mathcal{P}\mathcal{G}\mathcal{P}^T)^{-1}(\mathcal{P}\mathcal{G}\mathcal{P}^T) = \mathcal{G}\mathcal{P}^T - \mathcal{G}\mathcal{P}^T = 0$$

and

$$\mathcal{P}\mathcal{G}' = \mathcal{P}\mathcal{G} - (\mathcal{P}\mathcal{G}\mathcal{P}^T)(\mathcal{P}\mathcal{G}\mathcal{P}^T)^{-1}\mathcal{P}\mathcal{G} = \mathcal{P}\mathcal{G} - \mathcal{P}\mathcal{G} = 0,$$

which are (2.12). ∎

Using the expression (2.11) in (2.10), we see that the left-hand side of (2.10) is

$$(2.16) \qquad {}_{V^*}\langle \mathcal{L}\bar{u}, \bar{v}\rangle_V - {}_{V^*}\langle \mathcal{L}\mathcal{G}'\mathcal{L}\bar{u}, \bar{v}\rangle_V = {}_{\bar{V}^*}\langle (\mathcal{P}\mathcal{G}\mathcal{P}^T)^{-1}\bar{u}, \bar{v}\rangle_{\bar{V}}\,.$$

As $(\mathcal{P}\mathcal{G}\mathcal{P}^T)^{-1}$ is obviously invertible, (2.16) confirms that (2.10) is a well-posed formulation.

In the cases of practical interest, $\bar{V}$ is a finite-dimensional subspace of V. If the dimension of $\bar{V}$ is N, then we can find a set of functionals $\{\mu_i\}_{i=1,\dots,N}$ such that for all $v \in V$

$$ {}_{V^*}\langle \mu_i, v\rangle_V = 0 \quad \forall i = 1,\dots,N \qquad \Leftrightarrow \qquad \mathcal{P}v = 0. \tag{2.17}$$

In other words, the equations ${}_{V^*}\langle \mu_i, v\rangle_V = 0$ for $1 \le i \le N$ characterize v as a fine-scale function, i.e., $v \in V'$. From the mathematical standpoint, $\{\mu_i\}_{i=1,\dots,N}$ is a basis for the image of $\mathcal{P}^T$. Therefore, it is clear that (2.12) is equivalent to

$$ \mathcal{G}'\mu_i = 0 \qquad \forall i = 1,\dots,N \tag{2.18}$$

and

$$ {}_{V^*}\langle \mu_i, \mathcal{G}'\nu\rangle_V = 0 \qquad \forall \nu \in V^* \ \forall i = 1,\dots,N. \tag{2.19}$$

Moreover, after introducing the vector $\boldsymbol{\mu} \in (V^*)^N$ and its transpose,

$$ \boldsymbol{\mu} = \begin{bmatrix} \mu_1 \\ \vdots \\ \mu_N \end{bmatrix} \qquad \text{and} \qquad \boldsymbol{\mu}^T = \begin{bmatrix} \mu_1 & \dots & \mu_N \end{bmatrix}; $$

the vector $\mathcal{G}\boldsymbol{\mu}^T \in V^N$,

$$ \mathcal{G}\boldsymbol{\mu}^T = \begin{bmatrix} \mathcal{G}\mu_1 & \dots & \mathcal{G}\mu_N \end{bmatrix}; $$

the matrix $\boldsymbol{\mu}\mathcal{G}\boldsymbol{\mu}^T \in \mathbb{R}^{N\times N}$,

$$ \boldsymbol{\mu}\mathcal{G}\boldsymbol{\mu}^T = \begin{bmatrix} {}_{V^*}\langle \mu_1, \mathcal{G}\mu_1\rangle_V & \dots & {}_{V^*}\langle \mu_1, \mathcal{G}\mu_N\rangle_V \\ \vdots & \ddots & \vdots \\ {}_{V^*}\langle \mu_N, \mathcal{G}\mu_1\rangle_V & \dots & {}_{V^*}\langle \mu_N, \mathcal{G}\mu_N\rangle_V \end{bmatrix}; $$

and the vector of functionals $\boldsymbol{\mu}\mathcal{G} : (V^*) \to \mathbb{R}^N$ (i.e., $\boldsymbol{\mu}\mathcal{G} \in (V^{**})^N$) such that

$$ \boldsymbol{\mu}\mathcal{G}(\nu) = \begin{bmatrix} {}_{V^*}\langle \mu_1, \mathcal{G}\nu\rangle_V \\ \vdots \\ {}_{V^*}\langle \mu_N, \mathcal{G}\nu\rangle_V \end{bmatrix} \quad \forall \nu \in V^*, $$

it is easy to see that (2.11) is equivalent to

$$ \mathcal{G}' = \mathcal{G} - \mathcal{G}\boldsymbol{\mu}^T \left[\boldsymbol{\mu}\mathcal{G}\boldsymbol{\mu}^T\right]^{-1} \boldsymbol{\mu}\mathcal{G}. \tag{2.20}$$

2.4. Orthogonal projectors and optimization. An interesting case, and the only one considered in what follows, is when $\mathcal{P}$ is an orthogonal projector.

Given a scalar product $(\cdot,\cdot)$ defined on $V \times V$, possibly different than $(\cdot,\cdot)_V$, the related orthogonal projector $\mathcal{P}$ is obviously defined by

$$ (\mathcal{P}w, \bar{v}) = (w, \bar{v}) \qquad \forall w \in V, \forall \bar{v} \in \bar{V}. \tag{2.21}$$

Recall that, in order to fit in the abstract framework of section 2.2, $\mathcal{P}$ must be a continuous operator in V. However, when $\bar{V}$ is a finite-dimensional space, this holds for any scalar product $(\cdot,\cdot)$ which is continuous on $V \times V$.

In this context, V' and $\bar{V}$ are orthogonal complements with respect to $(\cdot,\cdot)$, and the VMS formulation provides the optimal approximation $\bar{u} \in \bar{V}$ of u, with respect to the norm $\|\cdot\|$ induced by the scalar product $(\cdot,\cdot)$.

3. The advection-diffusion model problem. Let d be the space dimension ($d = 1$ and $d = 2$ will be taken into consideration in the examples), and let $\Omega \subset \mathbb{R}^d$ be a regular domain. We consider the advection-diffusion model problem

$$\mathcal{L}u = -\kappa\Delta u + \beta \cdot \nabla u = f \text{ in } \Omega \qquad \text{with } u_{|\partial\Omega} = 0, \tag{3.1}$$

where $f \in L^2(\Omega)$ is the source term, $\kappa > 0$ is the scalar diffusivity, and $\beta : \Omega \to \mathbb{R}^d$ is the advection field, for which we assume $\mathrm{div}(\beta) = 0$. For the variational formulation of (3.1), within the framework of section 2, we set $V = H^1_0 \equiv H^1_0(\Omega)$ whence $V^* = H^{-1}$. Typical finite element spaces will be considered as coarse spaces $\bar{V}$.

In this context, it is convenient to represent the Green's operator $\mathcal{G}$ through the Green's function $g : \Omega \times \Omega \to \mathbb{R}$ such that

$$u(y) = \int_\Omega g(x, y) f(x)\, dx \tag{3.2}$$

for almost every y in Ω. Note that in (3.2) and in what follows the integrals have to be interpreted in the sense of distributions. We refer to [22] for details. Some explicit representations are given in [13].

We recall that $g_{|\partial(\Omega\times\Omega)} = 0$ and, for all $y \in \Omega$, $\mathcal{L}^* g(\cdot, y) = \delta(\cdot - y)$, where δ is the Dirac mass at the origin and $\mathcal{L}^* = -\kappa\Delta - \beta \cdot \nabla$ denotes the dual of $\mathcal{L}$.

Furthermore, we introduce the fine-scale Green's function $g' : \Omega \times \Omega \to \mathbb{R}$, which represents the fine-scale Green's operator $\mathcal{G}'$ and gives the fine-scale component u' of u from the coarse-scale residual $r = f - \mathcal{L}\bar{u}$ by

$$u'(y) = \int_\Omega g'(x, y) r(x)\, dx. \tag{3.3}$$

Recall, however, that the space of fine scales V' as well as the fine-scale Green's function g' depend on the underlying projector $\mathcal{P}$. With an abuse of notation, in the next sections we shall write V' and g' without distinction among the different projectors taken into consideration. In particular, we will deal with the H^1_0-projector $\mathcal{P} = \mathcal{P}_{H^1_0}$, associated with the scalar product $(w, v) = (w, v)_{H^1_0} = \int_\Omega \nabla w(x) \cdot \nabla v(x)\, dx$, and the usual L^2-projector $\mathcal{P} = \mathcal{P}_{L^2}$. Having a set of functionals $\{\mu_i\}_{i=1,\dots,N}$ as in (2.17), i.e., giving

$$\int_\Omega \mu_i(x) v(x)\, dx = 0 \quad \forall i = 1, \dots, N \qquad \Leftrightarrow \qquad \mathcal{P}v = 0, \tag{3.4}$$

then g' is obtained straightforwardly by (2.20) as

$$\begin{aligned} g'(x, y) =& g(x, y) - \left[\int_\Omega g(\tilde{x}, y)\mu_1(\tilde{x})\, d\tilde{x} \quad \cdots \quad \int_\Omega g(\tilde{x}, y)\mu_N(\tilde{x})\, d\tilde{x}\right] \\ & \times \begin{bmatrix} \int_\Omega g(\tilde{x}, \tilde{y})\mu_1(\tilde{x})\mu_1(\tilde{y})\, d\tilde{x}d\tilde{y} & \cdots & \int_\Omega g(\tilde{x}, \tilde{y})\mu_N(\tilde{x})\mu_1(\tilde{y})\, d\tilde{x}d\tilde{y} \\ \vdots & \ddots & \vdots \\ \int_\Omega g(\tilde{x}, \tilde{y})\mu_1(\tilde{x})\mu_N(\tilde{y})\, d\tilde{x}d\tilde{y} & \cdots & \int_\Omega g(\tilde{x}, \tilde{y})\mu_N(\tilde{x})\mu_N(\tilde{y})\, d\tilde{x}d\tilde{y} \end{bmatrix}^{-1} \\ & \times \begin{bmatrix} \int_\Omega g(x, \tilde{y})\mu_1(\tilde{y})\, d\tilde{y} \\ \vdots \\ \int_\Omega g(x, \tilde{y})\mu_N(\tilde{y})\, d\tilde{y} \end{bmatrix}, \end{aligned} \tag{3.5}$$

while (2.18) and (2.19) mean that, for all $x, y \in \Omega$ and for all $i = 1, \dots, N$,

$$\int_\Omega g'(\tilde{x}, y)\mu_i(\tilde{x})\, d\tilde{x} = 0 \text{ and } \int_\Omega g'(x, \tilde{y})\mu_i(\tilde{y})\, d\tilde{y} = 0. \tag{3.6}$$

In this context, the VMS formulation (2.10) reads as follows: Find $\bar{u} \in \bar{V}$ such that

$$\begin{aligned}\int_\Omega (\kappa \nabla \bar{u}(x) - \beta \bar{u}) \cdot \nabla \bar{v}(x)\, dx - \int_\Omega \int_\Omega \mathcal{L}\bar{u}(x) g'(x,y) \mathcal{L}^* \bar{v}(y)\, dxdy \\ = \int_\Omega f(x)\bar{v}(x)\, dx - \int_\Omega \int_\Omega f(x) g'(x,y) \mathcal{L}^* \bar{v}(y)\, dxdy \qquad \forall \bar{v} \in \bar{V}.\end{aligned} \tag{3.7}$$

3.1. Linear elements and H_0^1-optimality in one dimension. Let $d = 1$ and $\Omega = (0, L)$. Consider a grid of nodes $0 = x_0 < x_1 < \cdots < x_{n_{el}-1} < x_{n_{el}} = L$ and the related subdivision of $(0, L)$ into n_{el} elements (x_{i-1}, x_i), $i = 1, \ldots, n_{el}$. Let $\bar{V} \subset H_0^1$ be the space of piecewise-linear (with respect to the subdivision) functions, which is of dimension $N = n_{el} - 1$.

In this context, the H_0^1-projector $\mathcal{P} = \mathcal{P}_{H_0^1}$ plays a special role; indeed, $(\mathcal{P}v)(x_i) = v(x_i)$ for all $i = 1, \ldots, N$. Then, the VMS approach provides in this case a nodally exact approximation $\bar{u}$ of the exact solution u (see [3, 8, 12, 13]).

In order to have (3.4), we set $\mu_i = \delta(x - x_i)$. The abstract property (3.6) becomes, in this case,

$$g'(x, x_i) = g'(x_i, y) = 0 \qquad \forall i = 1, \ldots, N, \quad 0 \le x, y \le L; \tag{3.8}$$

i.e., g' vanishes if one of its two arguments is a node of the grid. Moreover, (3.5) gives

$$\begin{aligned}g'(x,y) = g(x,y) - \begin{bmatrix} g(x_1,y) & \cdots & g(x_N,y)\end{bmatrix} \\ \times \begin{bmatrix} g(x_1,x_1) & \cdots & g(x_N,x_1) \\ \vdots & \ddots & \vdots \\ g(x_1,x_N) & \cdots & g(x_N,x_N)\end{bmatrix}^{-1} \times \begin{bmatrix} g(x,x_1) \\ \vdots \\ g(x,x_N)\end{bmatrix}.\end{aligned} \tag{3.9}$$

Recalling that $\mathcal{L}^* g(\cdot, y) = \delta(\cdot - y)$, from (3.9) we get

$$\begin{aligned}\mathcal{L}^* g'(\cdot,y) = \delta(\cdot - y) - \begin{bmatrix} g(x_1,y) & \cdots & g(x_N,y)\end{bmatrix} \\ \times \begin{bmatrix} g(x_1,x_1) & \cdots & g(x_N,x_1) \\ \vdots & \ddots & \vdots \\ g(x_1,x_N) & \cdots & g(x_N,x_N)\end{bmatrix}^{-1} \times \begin{bmatrix} \delta(\cdot - x_1) \\ \vdots \\ \delta(\cdot - x_N)\end{bmatrix}.\end{aligned}$$

If $x_{i-1} < y < x_i$, then

$$\mathcal{L}^* g'(\cdot, y) = \delta(\cdot - y) \text{ in } (x_{i-1}, x_i), \tag{3.10}$$

while when $y > x_i$ or $y < x_{i-1}$,

$$\mathcal{L}^* g'(\cdot, y) = 0 \text{ in } (x_{i-1}, x_i). \tag{3.11}$$

This, with (3.8), fully characterizes g': By (3.8) and (3.11), we see that $g'(x, y) = 0$ if x and y belong to two different elements; moreover, (3.8) and (3.10) say that g' is, on each $(x_{i-1}, x_i) \times (x_{i-1}, x_i)$, the so-called *element* Green's function g^{el}, i.e., the Green's function for the restriction of $\mathcal{L}$ to the element (x_{i-1}, x_i), with homogeneous Dirichlet boundary conditions at the endpoints x_{i-1} and x_i. Since $g'(x, y) \neq 0$ only when x and y belong to the same element, (3.3) can be localized within each element

$$u'(y) = \int_{x_{i-1}}^{x_i} g'(x,y) r(x)\, dx \qquad \forall y \in (x_{i-1}, x_i). \tag{3.12}$$

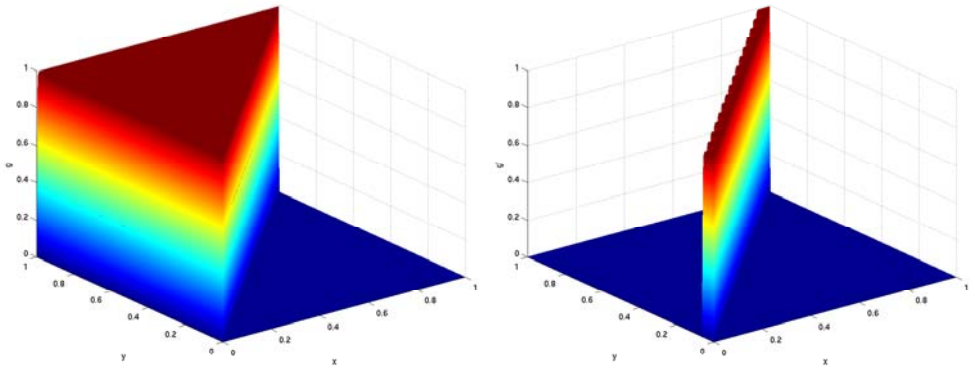

FIG. 3.1. *Comparison between the Green's function g (left) and the fine-scale Green's function g' (right) for the one-dimensional problem and linear elements, with $\mathcal{P} = \mathcal{P}_{H_0^1}$, $\kappa = 10^{-3}$, $\beta = 1$, $L = 1$, and a uniform grid of $n_{el} = 16$ elements. Note that the support of g' is local in that there is no coupling between elements. This is an advantage of $\mathcal{P} = \mathcal{P}_{H_0^1}$.*

See a plot of g' in Figure 3.1 where we consider the case of a uniform mesh of 16 elements (for $\kappa = 10^{-3}$, $\beta = 1$, and $L = 1$) and we compare with the plot of the Green's function g.

As stated above, the structure of g' for this case is well known in the literature [3, 8, 12, 13]. Indeed, recognizing that V' is the space of *bubbles*

$$V' = \bigoplus_{i=1,\dots,n_{el}} H_0^1(x_{i-1}, x_i), \tag{3.13}$$

the fine-scale variational equation (2.6) splits element by element and admits the strong form

$$\mathcal{L}u' = f - \mathcal{L}\bar{u} \text{ on } (x_{i-1}, x_i) \qquad \text{with } u'(x_{i-1}) = u'(x_i) = 0 \tag{3.14}$$

for each $i = 1, \dots, n_{el}$; u' is the solution of the advection-diffusion problem at the element level with the coarse-scale residual acting as the right-hand side. This is why $g' = g^{el}$ at the element level.

Moreover, assuming piecewise-constant coefficients κ, β and source term f, the fine-scale effect on the coarse-scale variational equation is

$$\begin{aligned} \int_0^L \int_0^L \mathcal{L}^* \bar{v}(y) g'(x,y) r(x)\, dxdy &= \sum_{i=1}^{n_{el}} \int_{x_{i-1}}^{x_i} \int_{x_{i-1}}^{x_i} \mathcal{L}^* \bar{v}(y) g'(x,y) r(x)\, dxdy \\ &= \sum_{i=1}^{n_{el}} \frac{\int_{x_{i-1}}^{x_i} \int_{x_{i-1}}^{x_i} g'(x,y)\, dxdy}{x_i - x_{i-1}} \int_{x_{i-1}}^{x_i} r(x) \mathcal{L}^* \bar{v}(x)\, dx, \end{aligned} \tag{3.15}$$

which is recognized as a classical stabilization term depending on the parameter [12, 13]

$$\tau_1 \equiv \tau_{1,(x_{i-1},x_i)} = \frac{\int_{x_{i-1}}^{x_i} \int_{x_{i-1}}^{x_i} g'(x,y)\, dxdy}{x_i - x_{i-1}} = \frac{h}{2\beta} \left(\coth(\alpha) - \frac{1}{\alpha} \right), \tag{3.16}$$

where $\alpha = (h\beta)/(2\kappa)$ is the mesh Peclét number and $h = x_i - x_{i-1}$ is the local mesh-size. We show plots of g' on the shifted element domain $(0, h) \times (0, h)$ in the diffusive and in the advective regime in Figure 3.2. A plot of τ_1 is presented in Figure 3.5.

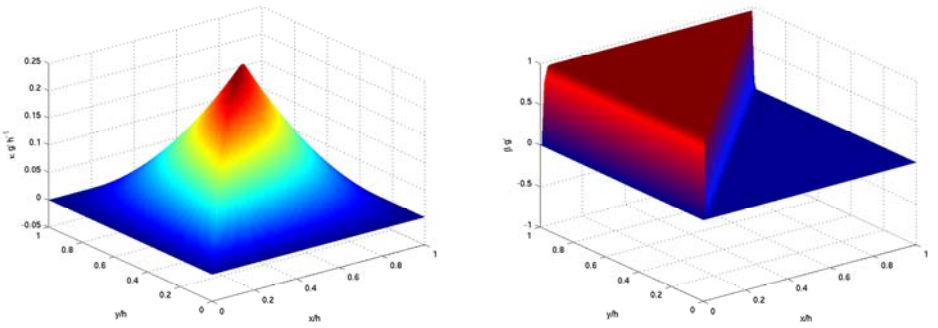

FIG. 3.2. *Fine-scale Green's functions g' at the element level $(0,h)\times(0,h)$ for the one-dimensional problem and linear elements. In the diffusive regime $\alpha = 10^{-2}$ (left), and in the advective regime $\alpha = 10^{2}$ (right). $\mathcal{P} = \mathcal{P}_{H_0^1}$.*

3.2. Higher-order elements and H_0^1-optimality in one dimension. We consider now higher-order piecewise-polynomial coarse scales on the grid $0 = x_0 < x_1 < \cdots < x_{n_{el}-1} < x_{n_{el}} = L$; i.e., we set

$$\bar{V} = \left\{\bar{v} \in H_0^1(0,L) \text{ such that } \bar{v}_{|(x_{i-1},x_i)} \in \mathbb{P}_k,\ 1 \le i \le n_{el}\right\},$$

where $\mathbb{P}_k$ is the space of polynomials of degree at most k. We still deal with $\mathcal{P} = \mathcal{P}_{H_0^1}$. The case of higher-order elements ($k \ge 2$) has not been studied in the literature of VMS methods, as far as we know. There are indeed additional difficulties with respect to the case of linear elements: V' is still a space of bubbles, but unlike the case $k = 1$, $\bar{V}$ also contains some (polynomial) bubbles, which are therefore missing in V'. This means that V' is a strict subset of bubbles

$$V' \subsetneq \bigoplus_{i=1,\ldots,n_{el}} H_0^1(x_{i-1},x_i), \tag{3.17}$$

or equivalently, V' is a space of bubbles with additional constraints. As a result, the fine-scale variational equation (2.6) can still be split element by element into

$$\int_{x_{i-1}}^{x_i} \mathcal{L}u'(x)v'(x)\,dx = \int_{x_{i-1}}^{x_i} (f(x) - \mathcal{L}\bar{u}(x))v'(x)\,dx \qquad \forall v' \in V', \quad i = 1,\ldots,n_{el}; \tag{3.18}$$

however, (3.18) is no longer equivalent to the strong form (3.14).

We can use the theory of section 2 for dealing with (3.18). Taking advantage of (3.17), we restrict from the beginning to a single element (x_{i-1},x_i) and to the bubbles supported on it. Then, we take as the fine-scale space $V_i' = V'_{|(x_{i-1},x_i)}$. The space of the bubbles which are polynomials of degree at most k plays the role of a coarse space on (x_{i-1},x_i); we set $\bar{V}_i = \bar{V}_{|(x_{i-1},x_i)} \cap H_0^1(x_{i-1},x_i)$. The space of unconstrained bubbles is $V_i = H_0^1(x_{i-1},x_i) = \bar{V}_i \oplus V_i'$. Precisely, $w \in V_i$ belongs to V_i' if and only if (integrating by parts)

$$0 = \int_{x_{i-1}}^{x_i} \frac{d}{dx}w(x)\frac{d}{dx}\bar{v}(x)\,dx = -\int_{x_{i-1}}^{x_i} w(x)\frac{d^2}{dx^2}\bar{v}(x)\,dx \qquad \forall \bar{v} \in \bar{V}_i. \tag{3.19}$$

The second-order derivatives of $\bar{V}_i$ functions are the polynomials of degree at most $k-2$. We need, as $\{\mu_j\}_{j=1,\ldots,N}$ (where $N = k-1$, now), a basis of $\mathbb{P}_{k-2}$. For example,

we can set $\mu_j(x) = (x - x_{i-1})^{j-1}$ for $1 \le j \le N$. The constraint is expressed, as in (2.17), by N scalar equations: $v \in V_i$ belongs to V_i' if and only if

$$\int_{x_{i-1}}^{x_i} \mu_j(x) v(x)\, dx = 0, \qquad 1 \le j \le N. \tag{3.20}$$

The Green's function of the unconstrained bubble problem is the element Green's function g^{el}. Then, we can use the formula (2.20) and derive an expression for g' in terms of g^{el}: on $(0,h)\times(0,h)$ we have

$$\begin{aligned} g'(x,y) = g^{el}(x,y) &- \begin{bmatrix} \int_0^h g^{el}(\tilde{x},y)d\tilde{x} & \cdots & \int_0^h \tilde{x}^{k-2} g^{el}(\tilde{x},y)d\tilde{x} \end{bmatrix} \\ &\times \begin{bmatrix} \int_0^h\int_0^h g^{el}(\tilde{x},\tilde{y})d\tilde{x}d\tilde{y} & \cdots & \int_0^h\int_0^h \tilde{x}^{k-2} g^{el}(\tilde{x},\tilde{y})d\tilde{x}d\tilde{y} \\ \vdots & \ddots & \vdots \\ \int_0^h\int_0^h \tilde{y}^{k-2} g^{el}(\tilde{x},\tilde{y})d\tilde{x}d\tilde{y} & \cdots & \int_0^h\int_0^h \tilde{x}^{k-2}\tilde{y}^{k-2} g^{el}(\tilde{x},\tilde{y})d\tilde{x}d\tilde{y} \end{bmatrix}^{-1} \\ &\times \begin{bmatrix} \int_0^h g^{el}(x,\tilde{y})d\tilde{y} \\ \vdots \\ \int_0^h \tilde{y}^{k-2} g^{el}(x,\tilde{y})d\tilde{y} \end{bmatrix}. \end{aligned} \tag{3.21}$$

We recall that $g'(x,y) = 0$ if x and y belong to different elements, while g' on each $(x_{i-1},x_i)\times(x_{i-1},x_i)$ can be obtained from (3.21) straightforwardly.

We discuss now in more detail the case of quadratic ($k = 2$) and cubic ($k = 3$) coarse-scale elements. If $k = 2$, then (3.21) yields

$$g'(x,y) = g^{el}(x,y) - \frac{\int_0^h g^{el}(\tilde{x},y)d\tilde{x}\int_0^h g^{el}(x,\tilde{y})d\tilde{y}}{\int_0^h\int_0^h g^{el}(\tilde{x},\tilde{y})d\tilde{x}d\tilde{y}}. \tag{3.22}$$

For $k = 3$, (3.21) gives

$$\begin{aligned} g'(x,y) = g^{el}(x,y) &- \begin{bmatrix} \int_0^h g^{el}(\tilde{x},y)d\tilde{x} & \int_0^h \tilde{x} g^{el}(\tilde{x},y)d\tilde{x} \end{bmatrix} \\ &\times \begin{bmatrix} \int_0^h\int_0^h g^{el}(\tilde{x},\tilde{y})d\tilde{x}d\tilde{y} & \int_0^h\int_0^h \tilde{x} g^{el}(\tilde{x},\tilde{y})d\tilde{x}d\tilde{y} \\ \int_0^h\int_0^h \tilde{y} g^{el}(\tilde{x},\tilde{y})d\tilde{x}d\tilde{y} & \int_0^h\int_0^h \tilde{x}\tilde{y} g^{el}(\tilde{x},\tilde{y})d\tilde{x}d\tilde{y} \end{bmatrix}^{-1} \\ &\times \begin{bmatrix} \int_0^h g^{el}(x,\tilde{y})d\tilde{y} \\ \int_0^h \tilde{y} g^{el}(x,\tilde{y})d\tilde{y} \end{bmatrix}. \end{aligned} \tag{3.23}$$

Plots of g' on $(0,h)\times(0,h)$ are shown in Figures 3.3 and 3.4. (See [17] for explicit formulas.)

Observe that, from (2.18)–(2.19), g' is L^2-orthogonal to $\mathbb{P}_{k-2}$ in both variables x and y on each $(x_{i-1},x_i)\times(x_{i-1},x_i)$. Still assuming that the coefficients κ and β are piecewise-constant and the source term f is a piecewise-polynomial of degree at most $k-1$, then on (x_{i-1},x_i) we have

$$r(x) = \frac{d^{k-1}r}{dx^{k-1}}\frac{x^{k-1}}{(k-1)!} + \text{ “polynomial of degree } \le k-2\text{”}$$

and

$$\mathcal{L}^*\bar{v}(y) = \frac{d^{k-1}\mathcal{L}^*\bar{v}}{dx^{k-1}}\frac{y^{k-1}}{(k-1)!} + \text{ “polynomial of degree } \le k-2\text{”}.$$

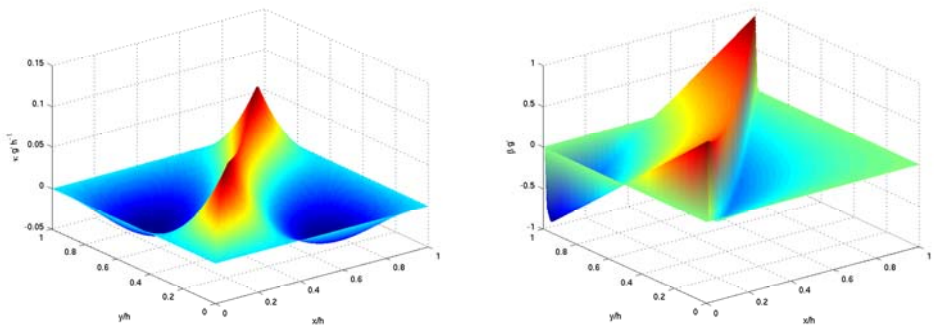

FIG. 3.3. *Fine-scale Green's functions g' at the element level $(0,h)\times(0,h)$ for the one-dimensional problem and quadratic elements. In the diffusive regime $\alpha = 10^{-2}$ (left), and in the advective regime $\alpha = 10^{2}$ (right). $\mathcal{P} = \mathcal{P}_{H_0^1}$.*

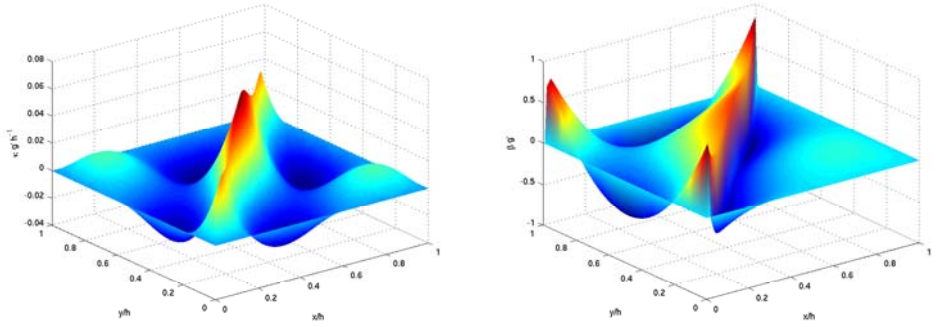

FIG. 3.4. *Fine-scale Green's functions g' at the element level $(0,h)\times(0,h)$ for the one-dimensional problem and cubic elements. In the diffusive regime $\alpha = 10^{-2}$ (left), and in the advective regime $\alpha = 10^{2}$ (right). $\mathcal{P} = \mathcal{P}_{H_0^1}$.*

Therefore, exploiting both the locality and the orthogonality of g' with respect to polynomials of degree $k-2$, the fine-scale effect on the coarse-scale equation can be written as

$$
\begin{aligned}
&\int_0^L \int_0^L \mathcal{L}^*\bar{v}(y) g'(x,y) r(x)\, dxdy \\
&\qquad = \sum_{i=1}^{n_{el}} \int_{x_{i-1}}^{x_i} \int_{x_{i-1}}^{x_i} \mathcal{L}^*\bar{v}(y) g'(x,y) r(x)\, dxdy \\
&\qquad = \frac{1}{((k-1)!)^2} \sum_{i=1}^{n_{el}} \int_{x_{i-1}}^{x_i} \int_{x_{i-1}}^{x_i} y^{k-1} \frac{d^{k-1}\mathcal{L}^*\bar{v}}{dx^{k-1}} g'(x,y) x^{k-1} \frac{d^{k-1} r}{dx^{k-1}}\, dxdy \\
&\qquad = \sum_{i=1}^{n_{el}} \frac{\int_{x_{i-1}}^{x_i}\int_{x_{i-1}}^{x_i} y^{k-1} g'(x,y) x^{k-1} dxdy}{((k-1)!)^2 (x_i - x_{i-1})} \int_{x_{i-1}}^{x_i} \frac{d^{k-1} r}{dx^{k-1}} \frac{d^{k-1}\mathcal{L}^*\bar{v}}{dx^{k-1}}\, dx \\
&\qquad = \sum_{i=1}^{n_{el}} \tau_{k,(x_{i-1},x_i)} \int_{x_{i-1}}^{x_i} \frac{d^{k-1} r}{dx^{k-1}} \frac{d^{k-1}\mathcal{L}^*\bar{v}}{dx^{k-1}}\, dx.
\end{aligned}
\tag{3.24}
$$

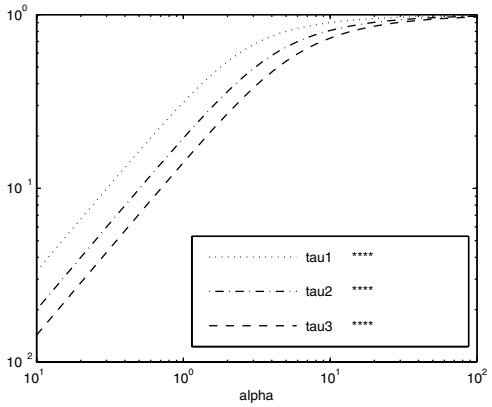

FIG. 3.5. *Stabilization parameters τ_1, τ_2, and τ_3 versus α.*

The stabilization term acts only locally and depends only on the derivative of degree $k-1$ of the residual; its effect is modulated by the parameter

$$\tau_k \equiv \tau_{k,(x_{i-1},x_i)} = \frac{\int_{x_{i-1}}^{x_i}\int_{x_{i-1}}^{x_i} y^{k-1}g'(x,y)x^{k-1}dxdy}{\left((k-1)!\right)^2(x_i - x_{i-1})}.$$

In the case of quadratic elements, from the previous formulas one can derive

$$\tau_2 = \frac{h^3}{72\,\beta}\frac{-3e^{2\alpha}\alpha^{-1} + e^{2\alpha} + 3e^{2\alpha}\alpha^{-2} - 3\alpha^{-2} - 1 - \alpha^{-1}}{e^{2\alpha} - e^{2\alpha}\alpha^{-1} + 1 + \alpha^{-1}},$$

while for cubic elements,

$$\tau_3 = \frac{h^5}{7200\,\beta}\,\frac{15e^{2\alpha}\alpha^{-2} - 6e^{2\alpha}\alpha^{-1} - 15e^{2\alpha}\alpha^{-3} + e^{2\alpha} + 15\alpha^{-3} + 6\alpha^{-1} + 15 + 1}{e^{2\alpha} - 3e^{2\alpha}\alpha^{-1} + 3e^{2\alpha}\alpha^{-2} - 1 - 3\alpha^{-2} - 3\alpha^{-1}}.$$

Plots of τ_1, τ_2, and τ_3 are compared in Figure 3.5.

Remark 1. From Figure 3.5 we see that the τ_k are positive and of order h^{2k-1}/β and $\alpha h^{2k-1}/\beta = h^{2k}/\kappa$ in the advective and in the diffusive regimes, respectively.

Remark 2. For linear elements, in one dimension, the H_0^1-optimal $\bar{u}$ is the nodal interpolant of u, which is a monotonicity preserving approximant. For higher-order elements, the H_0^1-optimal $\bar{u}$ is still nodally exact at the endpoints of each element, but we lose monotonicity inside the elements.

Remark 3. The format of (3.24) is reminiscent of the gradient least-squares stabilized method proposed by Franca and Dutra do Carmo [10].

3.3. L^2-optimality in one dimension and the localization of g'. We have shown that, for the one-dimensional problem and for the H_0^1-projector based VMS formulation (i.e., with $\mathcal{P} = \mathcal{P}_{H_0^1}$), the fine-scale Green's function is supported on the union of the $(x_{i-1}, x_i) \times (x_{i-1}, x_i)$ for $1 \le i \le n_{el}$. In this case, the g' is *fully localized* within each element, in that there is no coupling between elements. This allows a convenient evaluation of the fine-scale effect in the VMS formulation (see (3.15) and (3.24)). This feature, though, is not guaranteed for any projector $\mathcal{P}$. Take, e.g., the L^2-projector $\mathcal{P} = \mathcal{P}_{L^2}$, with piecewise-linear elements. We can still compute g' from (3.5), where now, in order to have (3.4), $\{\mu_i\}_{i=1,\dots,N}$ is a basis for $\bar{V}$ itself. For

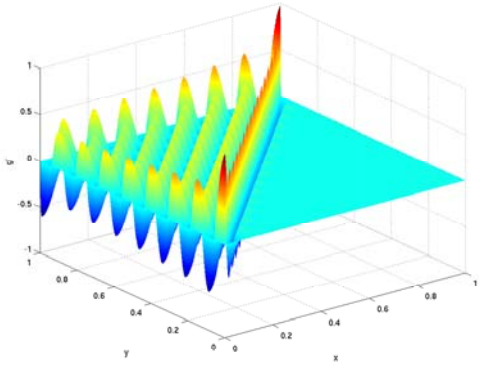

FIG. 3.6. *Fine-scale Green's function g' for the one-dimensional problem and linear elements, with $\mathcal{P} = \mathcal{P}_{L^2}$, $\kappa = 10^{-3}$, $\beta = 1$, $L = 1$, and a uniform grid of $n_{el} = 16$ elements. Note that in the case of $\mathcal{P} = \mathcal{P}_{L^2}$, g' is global and unattenuated when advection dominates.*

$\kappa = 10^{-3}$, $\beta = 1$, $L = 1$, and $n_{el} = 16$ elements, a plot of g' is presented in Figure 3.6; we see that the support of g' includes the entire upwind region $x \leq y$.

Remark 4. In practical applications, g' needs to be approximated, leading to classical stabilized methods. It is obviously more convenient and easy to approximate a highly localized g' than one that is global. This strongly suggests that the selection of the projector is crucial in the development of a multiscale method.

3.4. Linear elements in two dimensions. Turning to problems in two dimensions (as well as in multiple dimensions), we face two important differences.

First, it is technical and more difficult to obtain the analytical expression of the Green's function g and therefore of the fine-scale Green's function g' through (3.5). To overcome this difficulty, in this section we use the standard Galerkin method to numerically compute g and g' on a fine mesh of $524,288$ elements, which is able to resolve the fine scales of the problem under consideration.[1] We take here $\Omega = (0,1)^2$, the diffusivity is $\kappa = 10^{-3}$, and the unit advection velocity is $\beta = [1/2 \quad 1]/\sqrt{1.25}$. Since both g and g' are defined on $(0,1)^2 \times (0,1)^2$, for the purposes of a graphical representation we fix $y = y^* = [39/64 \quad 51/64] \approx [0.6 \quad 0.8]$ (see Figure 3.7), and we plot the Green's function g, and the fine-scale Green's function g' versus the argument x. The plot of $x \mapsto g(x, y^*)$ is presented in Figure 3.8. As is known, $x \mapsto g(x, y^*)$ is singular when $x = y^*$, and indeed the left graph in Figure 3.8 has been truncated at $g = 50$. Roughly speaking, g is supported around the upwind characteristic passing through y^*.

The second major difference, compared to the one-dimensional case, is that if the coarse scales are piecewise-polynomial, then the fine scales are not localized within each element (i.e., they are not bubble functions), and this happens for any choice of projector $\mathcal{P}$, including the H_0^1-projector. Indeed, since the coarse scales are polynomials on the edges of the elements of the triangulation, while the exact solution is arbitrary, the fine scales do not vanish there. Our aims here are the calculation of g'

[1] Let $\{\phi_i\}$ be a basis for piecewise-linear functions on the fine mesh, and think of $V \approx \text{span}\{\phi_i\}$, roughly speaking. Let $\mathbf{L}$ be the matrix representation of $\mathcal{L}$ (i.e., $L_{ij} = {}_{V^*}\langle \mathcal{L}\phi_j, \phi_i \rangle_V$), then the approximation of the Green's operator $\mathcal{G}$ is associated with $\mathbf{G} = \mathbf{L}^{-1}$. The approximation of $\mathcal{G}'$ in matrix form is obtained by $\mathbf{G}' = \mathbf{G} - \mathbf{G} \times \mathbf{P}^T \times (\mathbf{P} \times \mathbf{G} \times \mathbf{P}^T)^{-1} \times \mathbf{P} \times \mathbf{G}$, analogous to (2.11), where $\mathbf{P}$ is the matrix associated with the projector $\mathcal{P}$. The Green's function and fine-scale Green's function can be approximated as $g(x,y) \approx \sum_{i,j} G_{ij}\phi_j(x)\phi_i(y)$ and $g'(x,y) \approx \sum_{i,j} G'_{ij}\phi_j(x)\phi_i(y)$.

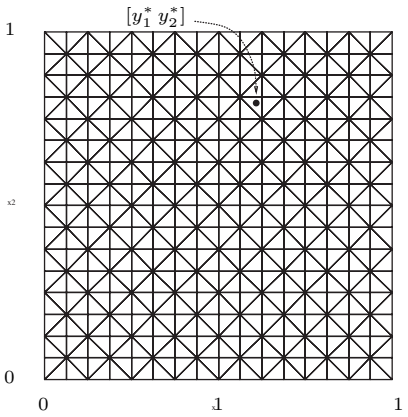

FIG. 3.7. *Mesh of the coarse-scale space $\bar{V}$ used for the calculation of the Green's functions in the two-dimensional case and the location of $y^* = [y_1^* \quad y_2^*]$.*

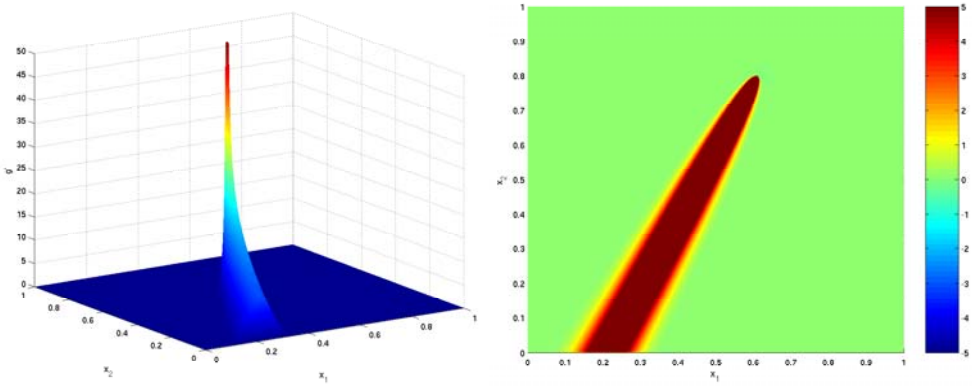

FIG. 3.8. *Plot (left) and contour plot (right) of $x \mapsto g(x, y^*)$.*

and the assessment of its attenuation compared with g and its locality for different choices of $\mathcal{P}$. We test both $\mathcal{P} = \mathcal{P}_{H_0^1}$ and $\mathcal{P} = \mathcal{P}_{L^2}$, which gave, in the one-dimensional case, a fully localized and a globally supported g', respectively. We take the space $\bar{V}$ formed by linear elements on the uniform triangulation shown in Figure 3.7. The plots of $x \mapsto g'(x, y^*)$ for $\mathcal{P} = \mathcal{P}_{H_0^1}$ and $\mathcal{P} = \mathcal{P}_{L^2}$ are presented in Figures 3.9 and 3.10, respectively. The singularity at $x = y^*$ is truncated at $g' = 50$ in the left-hand plots and at $g' = 5$ in the right-hand plots. Observe that in the case $\mathcal{P} = \mathcal{P}_{H_0^1}$, the fine-scale Green's function is more localized around y^*, compared with the case $\mathcal{P} = \mathcal{P}_{L^2}$, for which oscillations are spread over the entire domain. In addition, the g' for the case $\mathcal{P} = \mathcal{P}_{H_0^1}$ seems to be negligible outside a layer of a few elements around y^*. This is better seen in the (right-hand) contour plots of Figure 3.9 and 3.10, where the coarse mesh is overlaid.

Changing the position of y^* inside Ω and taking y^* on an edge or a vertex of the coarse triangulation produces similar results (not shown).

Remark 5. The upwind tail of g is global in the advection-dominated case, whereas it is highly attenuated for g' when $\mathcal{P} = \mathcal{P}_{H_0^1}$ (cf. Figure 3.8 with Figure 3.9). This has important implications for multiscale analysis of dominantly hyperbolic phenomena. In addition, the g' for $\mathcal{P} = \mathcal{P}_{H_0^1}$ is much more localized than that for

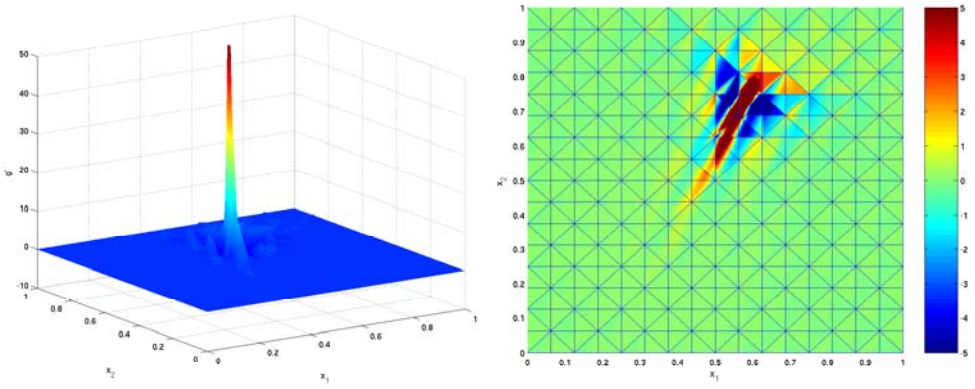

FIG. 3.9. *Plot (left) and contour plot (right) of* $x \mapsto g'(x, y^*)$ *for* $\mathcal{P} = \mathcal{P}_{H_0^1}$.

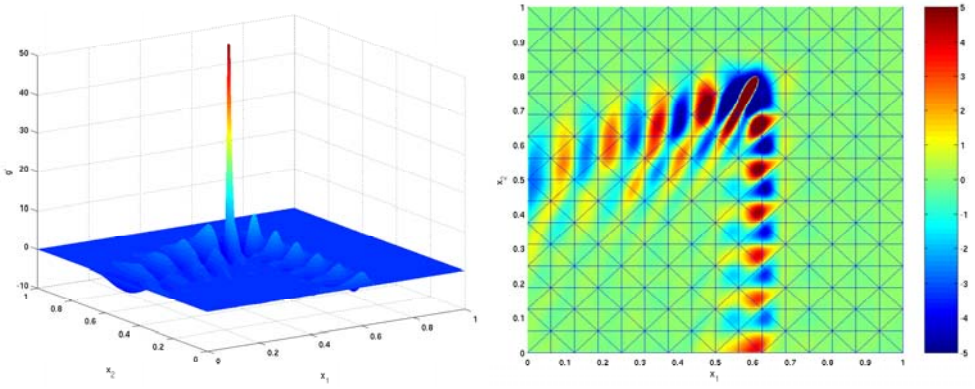

FIG. 3.10. *Plot (left) and contour plot (right) of* $x \mapsto g'(x, y^*)$ *for* $\mathcal{P} = \mathcal{P}_{L^2}$.

$\mathcal{P} = \mathcal{P}_{L^2}$. These results are consistent with the one-dimensional case and suggest that local approximations of g' for $\mathcal{P} = \mathcal{P}_{H_0^1}$ may achieve near H_0^1-optimality in multidimensional, advection-dominated cases.

Let us return to the model problem (3.1) with κ and β defined as above. We now consider a right-hand side $f = +1$ if $x_2 \geq 2x_1$, $f = -1$ if $x_2 < 2x_1$. The exact solution has an internal layer along $x_2 = 2x_1$, due to the discontinuity of f, and boundary layers at $x_1 = 1$ and $x_2 = 1$.

We consider three different meshes: The first two are shown in Figure 3.11, and the third is the same as the one depicted in Figure 3.7. The three meshes are quite coarse for the problem considered. The coarse-scale approximations $\bar{u}$ are given in Figures 3.12–3.14 for $\mathcal{P}_{H_0^1}$ and $\mathcal{P}_{L^2}$. In Figure 3.12 it is very clear that the solution for $\mathcal{P}_{H_0^1}$ is much better than that for $\mathcal{P}_{L^2}$. In Figure 3.13, the solution for $\mathcal{P}_{H_0^1}$ is better than that for $\mathcal{P}_{L^2}$ but not by as wide margin as in Figure 3.12. The trend continues in Figure 3.14, but the solution for $\mathcal{P}_{H_0^1}$ is only slightly better than that for $\mathcal{P}_{L^2}$. We have tested other meshes, obtaining results (not shown) similar to the ones of Figures 3.12–3.14. The superiority of $\mathcal{P}_{H_0^1}$ seems to be a general fact, though it is more apparent for finer meshes than coarser meshes. One might conclude that H_0^1-optimality is not as strong a condition as it is often thought to be and may not be enough in many practical cases for which monotonicity is deemed essential.

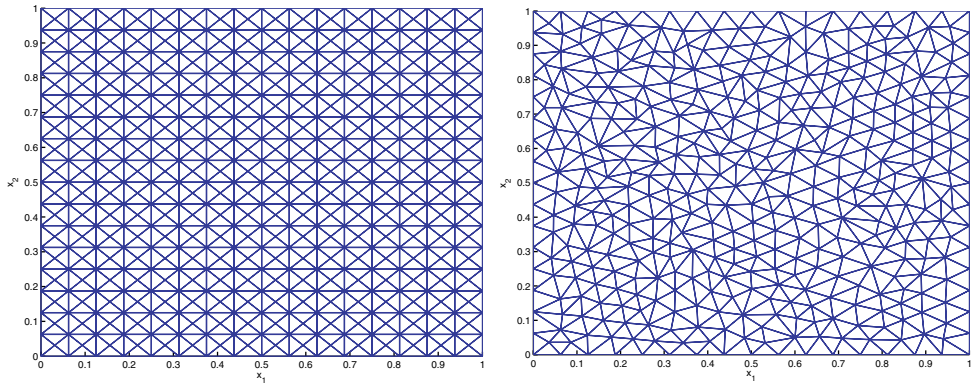

FIG. 3.11. *First two meshes associated with the coarse-scale spaces $\bar{V}$, used for the calculations of the coarse-scale components $\bar{u}$ of the model problem.*

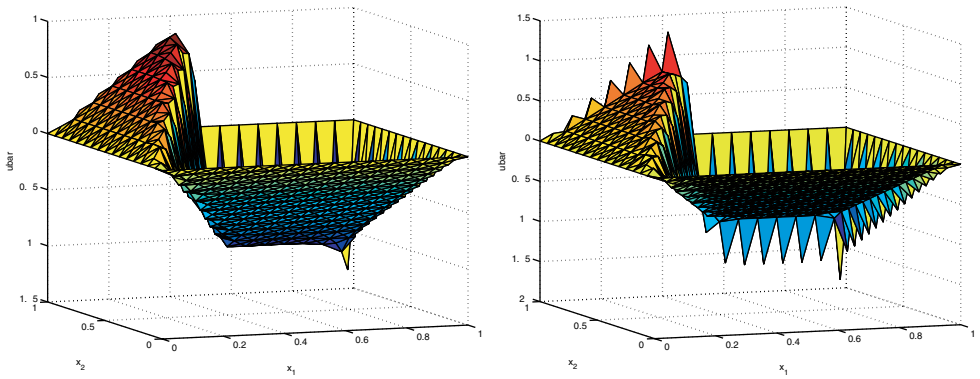

FIG. 3.12. *Coarse-scale component $\bar{u}$ for the model problem. $\mathcal{P} = \mathcal{P}_{H_0^1}$ (left) and $\mathcal{P} = \mathcal{P}_{L^2}$ (right). The coarse-scale space $\bar{V}$ is based on the left-hand mesh in Figure* 3.11.

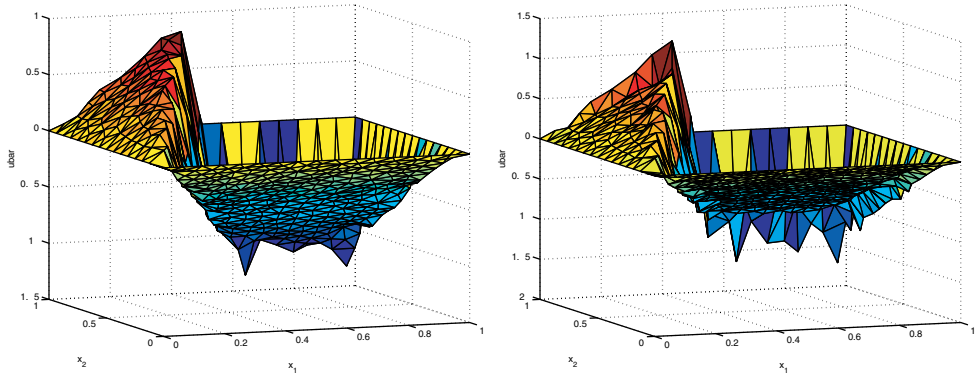

FIG. 3.13. *Coarse-scale component $\bar{u}$ for the model problem. $\mathcal{P} = \mathcal{P}_{H_0^1}$ (left) and $\mathcal{P} = \mathcal{P}_{L^2}$ (right). The coarse-scale space $\bar{V}$ is based on the right-hand mesh in Figure* 3.11.

Remark 6. In the case $\mathcal{P} = \mathcal{P}_{H_0^1}$, because of (3.6) we have, in the sense of distributions, $\int_\Omega g'(x,y)\Delta\bar{v}(y)\,dy = 0$ for all $\bar{v} \in \bar{V}$. Therefore, the fine-scale effect on

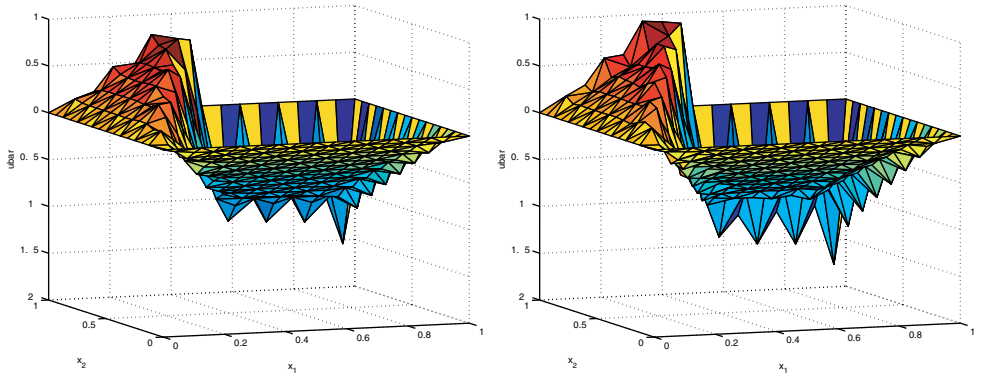

FIG. 3.14. *Coarse-scale component $\bar{u}$ for the model problem. $\mathcal{P} = \mathcal{P}_{H_0^1}$ (left) and $\mathcal{P} = \mathcal{P}_{L^2}$ (right). The coarse-scale space $\bar{V}$ is based on the mesh in Figure* 3.7.

the coarse-scale equation (3.7) becomes

$$\begin{aligned}\int_\Omega \int_\Omega \left(f(x) - \mathcal{L}\bar{u}(x)\right) g'(x,y) \mathcal{L}^* \bar{v}(y)\, dxdy \\ = -\int_\Omega \int_\Omega \left(f(x) - \mathcal{L}\bar{u}(x)\right) g'(x,y) \beta \cdot \nabla \bar{v}(y)\, dxdy.\end{aligned} \tag{3.25}$$

In one dimension, where g' is fully localized, the right-hand side of (3.25) is precisely the classical SUPG stabilization (see [9]); i.e., the residual is weighted only by the advective part of the operator, and the g' gives rise to the elementwise optimal τ, as described in sections 3.1 and 3.2. (Recall that f was assumed to be a piecewise-polynomial of degree at most $k-1$.) Note also that the diffusion operator in the residual in (3.25) may also be eliminated due to the aforementioned orthogonality property. These observations hold in higher dimensions as well, except g' is not fully localized within individual elements. In the classical multidimensional SUPG method [9], instead of (3.25) we have $-\sum_{e=1}^{n_{el}} \int_{\Omega_e} \left(f(x) - \mathcal{L}\bar{u}(x)\right) \tau(x)\, \beta \cdot \nabla \bar{v}(x)\, dx$, where Ω_e, $e = 1, \ldots, n_{el}$, are the elements of the mesh on Ω. The primary difference between SUPG and (3.25) is that g' is replaced by the elementwise constant τ. This approximation may be justified in light of the localized nature of g'. Indeed, SUPG has been shown to converge at optimal rates in higher dimensions (see, e.g., [19]), although in advection-dominated cases, the "stability" norm is not as strong as the H_0^1-seminorm in that it only contains the streamline derivative.

Remark 7. The residual-free bubble approach [4, 5, 6, 7, 8, 20, 21] has been shown in [3] to be equivalent to a multiscale method in which the fine-scale Green's function is approximated by a local element Green's function [12, 13]. Use of a local Green's function, in light of the framework described herein, can be rigorously justified only in the one-dimensional case in which the H_0^1-projector is employed. However, this amounts to a very convenient approximation in practice and one that is known to generate effective stabilized methods [1, 5, 6, 20]. With a better knowledge of g' in the multidimensional case, we would anticipate that improved stabilization schemes could be devised.

4. Conclusions. In this paper we have derived an expression for the fine-scale Green's function arising in VMS analysis. The specification of a projector, defining the direct-sum decomposition into coarse-scale and fine-scale components, renders the

problem for the fine-scale Green's function well-posed. Different projectors give rise to different fine-scale Green's functions, and their properties can vary considerably. It is felt to be beneficial if the fine-scale Green's function is more attenuated than the classical Green's function, and its support is dominantly local. It is found that the projector induced by the H_0^1-seminorm enjoys these properties whereas the projector induced by the L^2-norm does not.

The primary practical result of these studies is in the development of a framework for approximate multiscale methods. Indeed, in general it is not possible to exactly calculate the fine-scale Green's function. Despite its complexity, its orthogonality properties suggests simplified constructs in the form of stabilized methods. This is instantiated precisely in one dimension for the H_0^1-projector, and its possibility in higher dimensions is suggested as well. In fact, it is shown that the H_0^1-optimal method and SUPG have features in common.

The results obtained clarify the relationship between the fine-scale Green's function and the properties of the coarse-scale solution. However, we considered projectors associated only with inner products, and in particular, we studied only the H_0^1- and L^2-projectors. The coarse-scale solution achieves optimality in terms of the corresponding norm. One could conceive of requiring the coarse-scale solution to achieve optimality in other measures giving rise to nonlinear structure. This is an intriguing possibility in that one could, e.g., require monotonicity, or other desirable behavior. In the past, ad hoc procedures have been used to instill such properties in numerical methods, but the present ideas seem to have the potential for studying these issues in a more fundamental way.

Presently, most numerical methods are given as recipes, and they are evaluated ex post facto by the way they satisfy desired objectives. The present developments suggest a different approach: designing numerical methods to satisfy desired objectives ab initio. We are a long way from making this a practical reality, but we believe some small steps have been taken in this direction.

Acknowledgments. G. Sangalli thanks the Institute for Computational Engineering and Sciences (University of Texas at Austin) for kind hospitality. We thank Rich Lehoucq for insightful remarks and inspiration.

REFERENCES

[1] M. I. Asensio, A. Russo, and G. Sangalli, *The residual-free bubble numerical method with quadratic elements*, Math. Models Methods Appl. Sci., 14 (2004), pp. 641–661.

[2] F. Brezzi and M. Fortin, *Mixed and Hybrid Finite Element Methods*, Springer-Verlag, New York, 1991.

[3] F. Brezzi, L. P. Franca, T. J. R. Hughes, and A. Russo, $b = \int g$, Comput. Methods Appl. Mech. Engrg., 145 (1997), pp. 329–339.

[4] F. Brezzi, L. P. Franca, and A. Russo, *Further considerations on residual-free bubbles for advective-diffusive equations*, Comput. Methods Appl. Mech. Engrg., 166 (1998), pp. 25–33.

[5] F. Brezzi, T. J. R. Hughes, L. D. Marini, A. Russo, and E. Süli, *A priori error analysis of residual-free bubbles for advection-diffusion problems*, SIAM J. Numer. Anal., 36 (1999), pp. 1933–1948.

[6] F. Brezzi, D. Marini, and E. Süli, *Residual-free bubbles for advection-diffusion problems: The general error analysis*, Numer. Math., 85 (2000), pp. 31–47.

[7] F. Brezzi and L. D. Marini, *Augmented spaces, two-level methods, and stabilizing subgrids*, Internat. J. Numer. Methods Fluids, 40 (2002), pp. 31–46.

[8] F. Brezzi and A. Russo, *Choosing bubbles for advection-diffusion problems*, Math. Models Methods Appl. Sci., 4 (1994), pp. 571–587.

[9] A. N. Brooks and T. J. R. Hughes, *Streamline upwind/Petrov-Galerkin formulations for convection dominated flows with particular emphasis on the incompressible Navier-Stokes equations*, Comput. Methods Appl. Mech. Engrg., 32 (1982), pp. 199–259.

[10] L. P. Franca and E. G. Dutra do Carmo, *The Galerkin gradient least-squares method*, Comput. Methods Appl. Mech. Engrg., 74 (1989), pp. 41–54.
[11] J. Holmen, T. J. R. Hughes, A. A. Oberai, and G. N. Wells, *Sensitivity of the scale partition for variational multiscale large-eddy simulation of channel flow*, Phys. Fluids, 16 (2004), pp. 824–827.
[12] T. J. R. Hughes, *Multiscale phenomena: Green's functions, the Dirichlet-to-Neumann formulation, subgrid scale models, bubbles and the origins of stabilized methods*, Comput. Methods Appl. Mech. Engrg., 127 (1995), pp. 387–401.
[13] T. J. R. Hughes, G. R. Feijóo, L. Mazzei, and J.-B. Quincy, *The variational multiscale method—A paradigm for computational mechanics*, Comput. Methods Appl. Mech. Engrg., 166 (1998), pp. 3–24.
[14] T. J. R. Hughes, L. Mazzei, and K. E. Jansen, *Large eddy simulation and the variational multiscale method*, Comput. Vis. Sci., 3 (2000), pp. 47–59.
[15] T. J. R. Hughes, L. Mazzei, A. A. Oberai, and A. A. Wray, *The multiscale formulation of large eddy simulation: Decay of homogeneous isotropic turbulence*, Phys. Fluids, 13 (2001), pp. 505–512.
[16] T. J. R. Hughes, A. A. Oberai, and L. Mazzei, *Large eddy simulation of turbulent channel flows by the variational multiscale method*, Phys. Fluids, 13 (2001), pp. 1784–1799.
[17] T. J. R. Hughes and G. Sangalli, *Variational multiscale analysis: The fine-scale Green's function, projection, optimization, localization, and stabilized methods*, Technical report 05-46, The Institute for Computational Engineering and Sciences, Austin, TX, 2005.
[18] T. J. R. Hughes, G. N. Wells, and A. A. Wray, *Energy transfers and spectral eddy viscosity in large-eddy simulations of homogeneous isotropic turbulence: Comparison of dynamic Smagorinsky and multiscale models over a range of discretizations*, Phys. Fluids, 16 (2004), pp. 4044–4052.
[19] C. Johnson, U. Nävert, and J. Pitkäranta, *Finite element methods for linear hyperbolic problems*, Comput. Methods Appl. Mech. Engrg., 45 (1984), pp. 285–312.
[20] G. Sangalli, *Global and local error analysis for the residual-free bubbles method applied to advection-dominated problems*, SIAM J. Numer. Anal., 38 (2000), pp. 1496–1522.
[21] G. Sangalli, *Capturing small scales in elliptic problems using a residual-free bubbles finite element method*, Multiscale Model. Simul., 1 (2003), pp. 485–503.
[22] I. Stakgold, *Green's Functions and Boundary Value Problems*, Pure Appl. Math. (NY), 2, Wiley-Interscience, New York, 1998.